

Adaptive pathways of coral populations on the Great Barrier Reef

Mikhail V. Matz^{1*}, Madeleine J. H. van Oppen^{2,3}, Line K Bay³ and Eric A. Trembl²

¹ Department of Integrative Biology, University of Texas at Austin, 205 W 24th St. C0990, Austin, Texas 78712, USA

² School of BioSciences, University of Melbourne, Victoria 3010 Australia

³ Australian Institute of Marine Science, QLD, Australia

* Author for correspondence, matz@utexas.edu

Abstract

Global warming is predicted to drive preferential survival of warm adapted genotypes that have migrated to cooler locations, and result in an overall decline in genetic diversity due to bleaching-related mortality. Population genomic analysis of *Acropora millepora* on the Great Barrier Reef (GBR) revealed that most populations were demographically distinct with preferential southward migration from lower (warmer) to higher (cooler) latitudes. Still, no recent increase in southward migration was detectable, and predicted migration rates remained closely correlated with those derived from a biophysical model based on ocean currents. There was also no evidence of recent declines in genetic diversity. A multi-locus adaptation model suggested that standing genetic variation spread across latitudes might be sufficient to fuel continuous adaptation of *A. millepora* metapopulation over 100-200 years of gradual warming. However, the model also predicts increase in severity of local mortality events induced by thermal anomalies, such as high bleaching-induced mortality in the northern GBR in 2016.

One-sentence summary: Patterns of migration and genetic diversity in a Great Barrier Reef coral favor efficient adaptation to gradual warming but do not alleviate the threat of bleaching and mortality from acute thermal extremes.

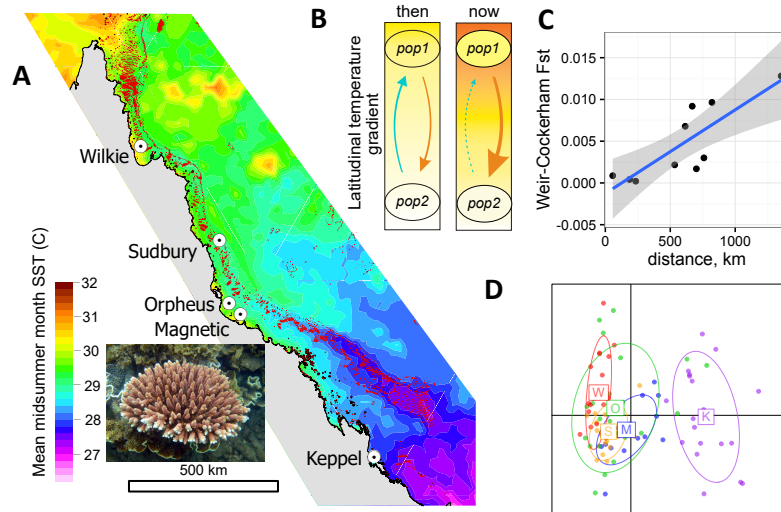
Hot water coral bleaching, caused by global warming, is devastating coral reefs around the world (1) but there is room for hope if corals can adapt to increasing temperatures. Many coral species have wide distributions that span environments that differ dramatically in their thermal regimes, demonstrating that efficient thermal adaptation has occurred in the past (2). But can coral adaptation keep up with the unprecedentedly rapid current rate of global warming (3)? One way for corals to achieve rapid thermal adaptation is through genetic rescue, involving the spread of existing heat tolerance alleles from low-latitude, warm-adapted populations to higher-latitude, warming regions, via larval migration (4, 5). We have previously demonstrated the presence of genetic variants conferring high thermal tolerance in a low-latitude *A. millepora* population (4). It

40 can be expected that global warming will cause preferential survival of warm-adapted poleward
41 migrants because they will be following their thermal optimum, whereas individuals migrating in
42 the opposite direction would find themselves in increasingly mismatched environments (Fig. 1 A,
43 B). Another likely population-level effect of recent declines in coral cover (6) is a reduction in
44 overall genetic diversity, potentially limiting both the scope and the rate of adaptation.

45
46 Here, we test these predictions in *Acropora millepora*, a common reef-building coral from the
47 most ecologically prominent and diverse coral genus in the Indo-Pacific (staghorn corals,
48 *Acropora*). We have analyzed genome-wide genetic variation using 2bRAD (7) in five
49 populations of *A. millepora* along the latitudinal range of the GBR (Fig. 1 A). We genotyped 18-
50 28 individuals per population at >98% accuracy and with a >95% genotyping rate. Analysis of
51 population structure based on ~11,500 biallelic SNPs separated by at least by 2,500 bases agreed
52 with previous microsatellites results (8, 9), and revealed very low levels of genetic divergence,
53 with only the Keppel Islands population being potentially different from the others (Fig. 1 D and
54 Fig. S1). We observed increasing genetic divergence with geographical distance (“isolation by
55 distance”, Fig. 1 C) that supports population divergence, however, pairwise F_{ST} were small and
56 did not exceed 0.014 even between the southernmost and northernmost populations (Keppel and
57 Wilkie). To gain a deeper insight into coral demography, we used Diffusion Approximation for
58 Demographic Inference (*dadi*, (10)) to more rigorously test for population subdivision and infer
59 pairwise migration rates among populations and population sizes. *dadi* is a coalescent-based
60 method that optimizes parameters of a pre-specified demographic model to maximize the
61 likelihood of generating the observed allele frequency spectrum (for two populations it is
62 essentially a two-dimensional histogram of allele frequencies, Fig. S2). Being a likelihood-based
63 method, *dadi* can be used to compare alternative models using likelihood ratio tests and Akaike
64 Information Criterion (AIC).

65
66 We used AIC to confirm that our populations are separate demographic units. For each pair of
67 populations we generated 120 bootstrapped datasets by resampling genomic contigs and
68 performed delta-AIC comparison of two demographic models, a split-with-migration model and a
69 no-split model (Fig. S3 B). The split-with-migration model assumed two populations that have
70 split some time T in the past, potentially have different sizes $N1$ and $N2$, and exchange migrants
71 at different rates ($m12$ and $m21$) depending on direction. The no-split model allowed for ancestral
72 population size to change at time T but not for a population split, so the experimental data were
73 modeled as two random samples from the same population of size N . The majority of bootstrap
74 replicates (88-100%) showed AIC advantage of the split-with-migration model for all but one
75 pair of populations (Sudbury-Magnetic, 39% bootstrap support; Fig. S3). This indicates that the
76 populations are demographically distinct despite very low F_{ST} . This result highlights the power of
77 coalescent analysis relative to classical approaches (such as F_{ST}) that assume genetic equilibrium,
78 i.e., that populations have been stable for thousands of generations.

79



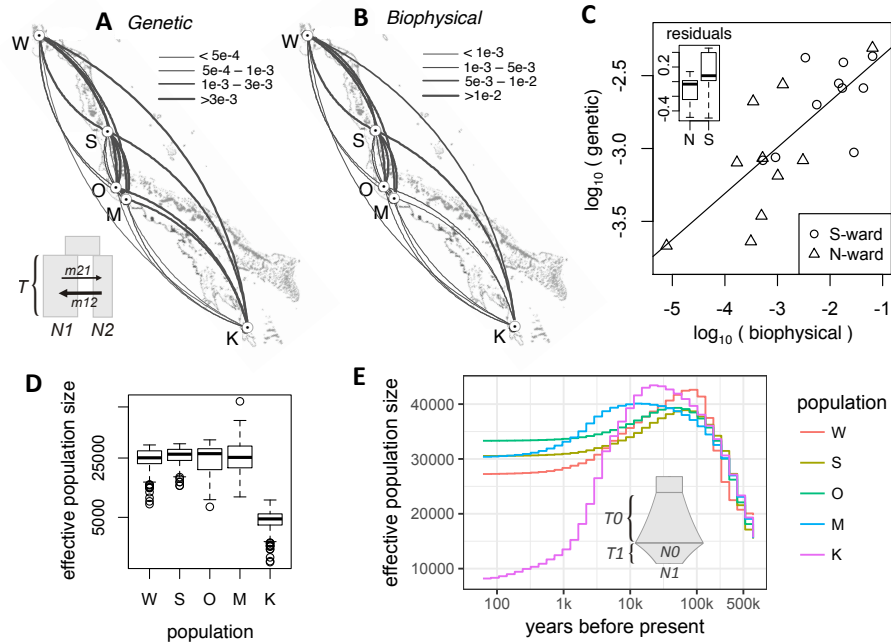
80
81 **Figure 1.** The population setting and background for our study. (A) Locations of sampled populations
82 where mean midsummer month sea surface temperature differed by up to $\sim 3^{\circ}\text{C}$. Inset: *Acropora millepora*.
83 (B) Working hypothesis under global warming: Warm-adapted low-latitude genotypes that migrate to
84 higher latitudes would be following their physiological optimum and hence expected to survive better than
85 migrants in the opposite direction. (C) Increase of pairwise F_{ST} with distance, both indicating weak genetic
86 divergence along the GBR, and (D) principal component analysis of genome-wide genetic variation. On
87 panel D, centroid labels are initial letters of population names as in panel A.
88

89 We then determined pairwise migration rates from the split-with-migration model and estimated
90 their confidence limits from bootstrap replicates. For all pairwise analyses except Wilkie-Sudbury
91 migration in southward direction exceeded northward migration, and this difference was
92 significant in seven out of nine cases (Fig. 2 A and Fig. S3A). Linear mixed model analysis of
93 direction dependent mean migration rates with a random effect of destination (to account for
94 variation in total migration rate) confirmed the overall significance of this southward trend
95 ($P_{\text{MCMC}} < 1e-4$).
96

97 It is important to note that our pairwise migration rates captured the cumulative effect of genetic
98 exchange between populations, which included direct migration and the spread of alleles via other
99 stepping-stone populations. Such rates do not directly reflect the numbers of larvae exchanged
100 between populations but are very informative in the genetic rescue context. They represent the
101 per-generation rate of replacement of the destination population genotypes by genotypes from the
102 source population, which is essentially the rate at which genetic rescue could proceed.
103

104 To investigate whether the southward migration bias was due to higher survival of southward
105 migrants relative to northward migrants, as predicted under global warming (Fig. 1 B), we
106 developed a biophysical model of coral larval dispersal on the Great Barrier Reef. This model

107 quantified the per-generation migration potential among coral reef habitat patches in the GBR
 108 based on ocean currents and parameters of larval biology (11, 12). We found that the genetic and
 109 biophysical migration rates were very closely correlated (Mantel test: $r = 0.79$, $P = 0.008$, Fig. 2
 110 C). Although the biophysical model explained most of the southward migration bias in the
 111 genetic data, the residuals were still in favor of southward migration (Fig. 2 C, inset; $P = 0.058$).
 112 While this residual excess suggest preferential survival of southward migrants, as predicted by
 113 our hypothesis (Fig. 1 B). These genetic predictions represent historical averages since the
 114 populations split and did not resolve any potential recent migration changes.



115
 116
 117 **Figure 2.** Demography of *A. millepora* populations on the GBR. (A) Arc-plot of migration rates among
 118 populations reconstructed from population genetic data. Inset: *dadi* model used: ancestral population splits
 119 into two populations of unequal sizes (N1 and N2) some time T in the past, these populations exchange
 120 migrants at different rates depending on direction. (B) Migration rates according to the biophysical model.
 121 On panels A and B, the arcs should be read clockwise to tell the direction of migration; line thickness is
 122 proportional to the migration rate. (C) Correlation between log-transformed biophysical and genetic
 123 migration rates (Mantel $r = 0.79$, $P = 0.008$). Inset: box-plot of residuals from the linear regression.
 124 Southward migration tends to exceed northward migration even after accounting for predictions of the
 125 biophysical model ($P = 0.058$), suggesting higher survival of southward migrants. (D) Box plot of effective
 126 population sizes inferred by the split-with-migration model (panel A) across all population pairs and
 127 bootstrap replicates. (E) Historical changes in effective population sizes inferred using a single-population
 128 *dadi* model with two periods of exponential growth (T0 and T1, reaching sizes N0 and N1, inset), averaged
 129 across bootstrap replicates.
 130

131 To determine any recent changes in southward migration, we evaluated a similar basic split-with-
132 migration model (Fig. 2A) that allowed for a change in migration over the past 75-100 years. The
133 new model suggested some recent migration changes, but there was no consistent change between
134 northward and southward migration (Fig. S4). Delta-AIC bootstrap analysis favored the new
135 model over the basic one only for two pairs of populations, Wilkie-Orpheus and Wilkie-Magnetic
136 (85 and 60% bootstrap support, respectively). We conclude that with the current data and analysis
137 techniques we cannot yet detect the effect of recent warming on preferential direction of coral
138 migration along the GBR.

139

140 The GBR has already warmed by 0.8°C since the end of last century (13) and may have already
141 reduced genetic diversity in *A. millepora* populations. We used *dadi* to infer effective population
142 sizes, which is a measure of genetic diversity and one of the key parameters determining the
143 population's adaptive potential (14). The results of the split-with-migration model (Fig. 2 A)
144 were consistent for all population pairs and indicated that Keppel population was about one-fifth
145 the size of others (Fig. 2 D, E). This result was not surprising since the Keppel population
146 frequently suffers high mortality due to environmental disturbances and was therefore is expected
147 to show diminished long-term effective population size (8). We also used a single-population
148 *dadi* model that allowed for two consecutive growth/decline periods (Fig. 2 E, inset) to
149 reconstruct effective sizes of individual populations through time (Fig. 2 E and Fig S5). All
150 populations showed evidence of growth prior to the last glaciation, 500-20 thousand years ago
151 (Fig 2 E), which aligned well with the fossil record of rising dominance of *Acropora* corals on
152 Indo-Pacific reefs during this period (15). It has been suggested that the fast growth and early
153 sexual maturation of *Acropora* corals gave them an advantage relative to most other reef-building
154 corals during dynamic changes in the reef-forming zone due to the sea level changes
155 accompanying glacial cycles (15). Our results suggest that *A. millepora* populations have been in
156 stasis or slow decline since sea level changes abated (Fig. S5), although the inclusion of an
157 additional growth/decline period only improved the model fit significantly for the Keppel
158 population (Fig S6). None of the populations showed evidence of accelerated decline in effective
159 population size over the past few hundred years. Although our samples were collected in the
160 early-mid 2000s, our results are still relevant since they characterize populations only two-three
161 coral generations ago. Disturbances that have affected corals since then would not yet have
162 substantially impacted genetic diversity.

163

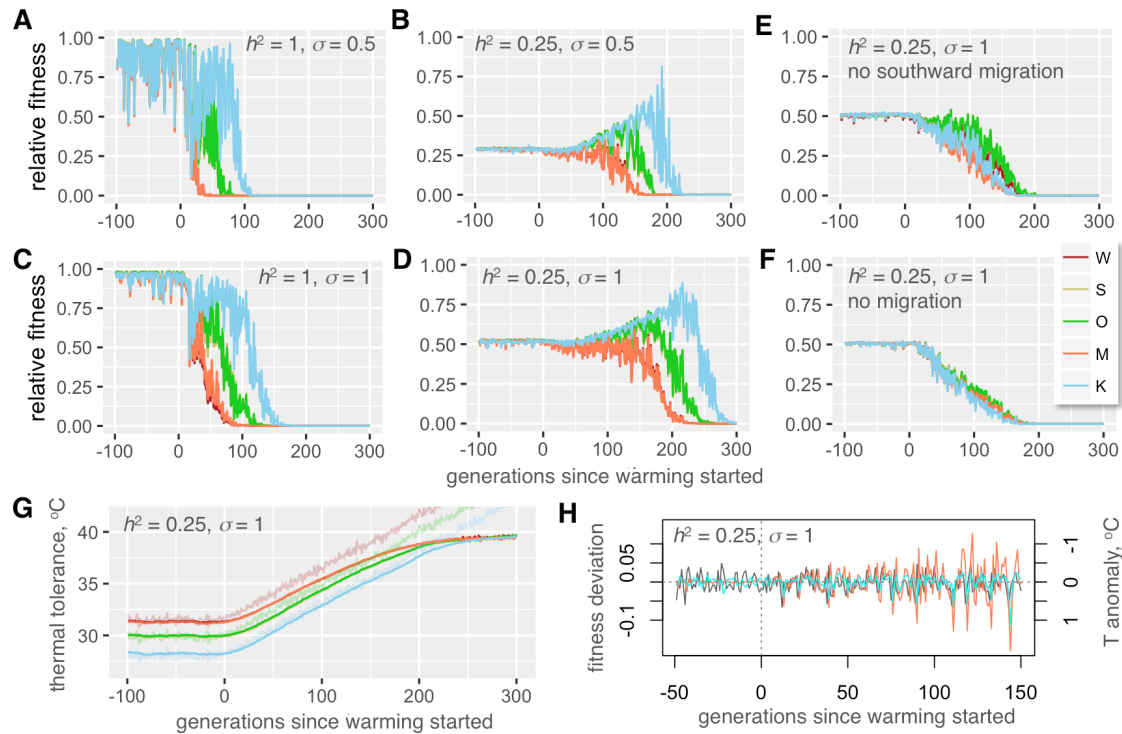
164 To evaluate whether standing genetic variation contributed by local thermal adaptation could
165 sustain evolution of the *A. millepora* metapopulation in response to warming, we have developed
166 a multi-QTL model of metapopulation adaptation in SLiM (16). The model was parameterized
167 with population sizes and migration rates inferred from the genetic analysis (Fig. 2 A, D), and
168 with differences in midsummer monthly mean temperature among populations (Fig. 1 A). The
169 number of QTLs and their effect sizes, phenotypic plasticity (standard deviation of the Gaussian
170 slope of fitness decline when phenotype mismatches the environment) and heritability (proportion

171 of phenotypic variation attributable to genetics) can all be varied in the model. It can also
172 incorporate climate scenarios with any combination of directional, cyclical and random changes.
173 The model also allows for new mutations but here the new mutation rate was set to zero. This was
174 to assess the contribution of only the standing genetic variation that was introduced into
175 populations at the start of simulation as random QTL effects. The climate scenario started with a
176 pre-adaptation to local thermal conditions for 2,000 generations. Assuming a generation time of
177 of 5 years in *A. millepora* (17) this corresponded to the period of stable temperature since the last
178 deglaciation. After pre-adaptation, the temperature was increased at a rate of 0.05°C/generation in
179 all populations, corresponding to the projected 0.1°C warming per decade (18). Throughout the
180 simulation temperature was allowed to fluctuate randomly between generations to approximate El
181 Nino Southern Oscillation (ENSO): the temperature deviations were drawn from a normal
182 distribution with a standard deviation of 0.25°C. The size of populations was kept constant
183 throughout the pre-adaptation period and scaled linearly with the populations' relative fitness
184 (mean current fitness divided by the mean fitness at the end of pre-adaptation period) during
185 warming. Migration rates from a population also scaled linearly with the population's fitness. In
186 this way, a population declining in fitness would shrink in size and stop contributing migrants to
187 other populations.

188
189 Our model suggested that, with only ten thermal QTLs, under all combinations of heritability and
190 plasticity the pre-adapted metapopulation would be able to persist through the warming for at
191 least 50-100 generations and, in some realistic cases, much longer (Fig. 3 and Figs. S7-S8).
192 Migration in general and southward migration in particular substantially contributed to this
193 persistence (Fig. 3 E, F), underscoring the importance of the spread of warm-adapted genotypes
194 from lower to higher latitudes (4).

195
196 Predictably, higher phenotypic plasticity promoted population persistence and stability against
197 random thermal anomalies, but we were rather surprised to observe a similar positive effect of
198 lower heritability, set to the values observed in coral quantitative genetics experiments (0.25-0.5,
199 (17); Fig 3, Fig. S7). One specific reason why corals are expected to show low heritability of
200 thermal tolerance is that much of natural variation in this trait in corals is due to the type of algal
201 symbionts (*Symbiodinium* spp. (19)). Photo-symbionts are not transmitted from parent to
202 offspring in the majority of coral species (20), and although host genetics can have some effect on
203 the choice of *Symbiodinium* in the next generation (21) environment has a very strong effect on
204 this association (19, 22). Higher persistence under low heritability and high plasticity is most
205 likely explained by the fact that they both allow for higher standing genetic variation to be
206 retained in populations (Fig. S9). During warming, this variation lasts longer as a source of
207 adaptive genetic variants, enabling up to 5°C increase in mean thermal tolerance over 150
208 generation (Fig. 3 G and Fig. S7). Higher plasticity partially rescued the drop in fitness due to low
209 heritability (Fig. 3 B and D, Fig. S7). Another notable tendency observed with all parameter
210 settings was that during warming the fitness (and hence the size) of adapting populations began to

211 fluctuate following random thermal anomalies, and the amplitude of these fitness fluctuations
 212 increased as the warming progressed even though the amplitude of thermal anomalies did not
 213 change (Fig. 3 H). These fluctuations correspond to severe mortality events induced by thermal
 214 extremes due to ENSO and affected warm-adapted populations most, which very much resembles
 215 the situation currently observed throughout the world (1).
 216



217
 218 **Figure 3.** Modeling coral metapopulation persistence under global warming. (A-D) Fitness of modeled
 219 populations depending on heritability of thermal tolerance (h^2 , proportion of tolerance variation explained
 220 by genetics), phenotypic plasticity (σ , standard deviation of the Gaussian slope of fitness decline away from
 221 the phenotypic optimum, in degrees C), and presence-absence of migration (E, F). On panels A-F, y-axis is
 222 observed fitness relative to maximal fitness at the genetically determined optimum, averaged over all
 223 individuals in a population. Warm-adapted populations (W and M) are shown as red-tint traces, populations
 224 from mild thermal regime (S and O) are green-tint traces, and the cool-adapted population (K) is the blue
 225 trace. Note nearly complete overlap between traces for pairs of populations pre-adapted to the same
 226 temperature (W,M and S,O). (G) Thermal tolerances of evolving populations. Thin noisy lines are modeled
 227 temperatures at different locations. (H) Modeled random temperature anomalies (grey line) and fluctuations
 228 in populations' fitness (the colored lines are residuals from loess regression over fitness traces on panel D;
 229 Wilkie: orange line, Keppel: blue line). Note the inverse sign of temperature anomalies: this more clearly
 230 shows the correspondence between rise in temperature and drop in fitness in the next generation. As
 231 warming progresses, populations (especially originally warm-adapted ones) become increasingly sensitive
 232 to random temperature fluctuations.
 233

234 There are several uncertainties in our model associated with coral biology. Higher number of
235 QTLs and/or their larger effect sizes would promote higher genetic variation and lead to longer
236 population persistence. To keep the analysis conservative, our model included only ten QTLs,
237 which is likely much fewer than the actual number of thermal QTLs in acroporid corals (20). We
238 also kept the distribution of QTL effect sizes narrow: with the current settings and ten QTLs, at
239 the start of simulation only about 2% of corals deviated from the mean thermal tolerance by more
240 than 1.5°C in either direction. Such narrow variation makes adaptation to the thermal gradient of
241 ~3°C along the GBR non-trivial, but still, at present there is no experimental data to evaluate
242 whether even such narrow variation is realistic. Our model was also conservative in using
243 effective population sizes suggested by genetic analysis as census sizes. In highly fecund marine
244 organisms census sizes tend to substantially exceed effective population sizes, sometimes by
245 orders of magnitude (23), which would strongly promote higher genetic diversity and population
246 persistence. Moreover, we modeled only our five populations rather than the whole GBR, which
247 would have resulted in much higher standing genetic variation in the metapopulation, promoting
248 longer persistence.

249
250 As for phenotypic plasticity, in simulations shown on Fig. 3, $\sigma = 0.5$ and $\sigma = 1$ corresponded to
251 86% and 40% decline in fitness if the individual's phenotype mismatched the environment by
252 1°C. The existing data on the issue of coral thermal plasticity are somewhat conflicting. One
253 study shows that acroporid corals can successfully acclimatize to environments differing in
254 maximum temperatures by as much as 2°C (24); however, another study found that coral grew
255 52-80% more slowly when transplanted among locations differing by 1.5°C average temperature,
256 (25). Although it is not possible to directly place these results into our quantitative plasticity
257 framework, the former study supports the higher plasticity setting ($\sigma = 1$) while the latter study
258 supports $\sigma = 0.5$. It must also be noted that both these studies involved *in situ* transplantations and
259 hence the effect of temperature remains confounded with other local fitness-affecting
260 environmental parameters. Also, in adult corals plasticity is likely lower than in larvae and
261 recruits, which are expected to exhibit non-reversible developmental plasticity associated with
262 metamorphosis and establishment within a novel environment (26). Future experiments that
263 expose multiple genetically distinct coral individuals to a range of temperatures under controlled
264 laboratory settings are required to rigorously quantify variation in thermal optima and plasticity in
265 natural populations.

266
267 In conclusion, we found that genetic diversity and migration patterns of our study species were
268 not yet affected by global warming and were well positioned to facilitate persistence of the GBR
269 metapopulation for a century or more. However, local mortality events induced by thermal
270 anomalies will be increasingly severe, especially among the originally warm-adapted populations.
271 The 10-85% mortality in the Northern GBR as a result of 2016 bleaching event (27) could be a
272 particularly sobering recent manifestation of this trend.

273

274 More research into phenotypic plasticity and genetic variation in coral thermal tolerance and its
275 genetic architecture (number of QTLs and their effect sizes) is needed to further improve the
276 predictive power of our model. The estimated migration in the order of 10 - 100 migrants per
277 generation could be feasibly facilitated by assisted gene flow efforts (28) without risking
278 disruption of the natural local adaptation patterns (29). Corals are declining on reef world-wide
279 and there is an urgent need to develop new solutions to effectively manage the impacts of global
280 processes such as climate change at local management scales. The broad characterization of
281 genetic diversity, local thermal adaptation and migration pathways in multiple reef-building coral
282 species would greatly inform both traditional spatial management and novel assisted gene flow
283 approaches and should therefore be given high priority.

284

285 **Methods**

286

287 *Genotyping*

288

289 This study relied predominantly on samples described by van Oppen et al (9), with addition of
290 several samples from Orpheus and Keppel islands that were used in the reciprocal transplantation
291 experiment described by Dixon et al (30). The samples were genotyped using 2bRAD (7)
292 modified for Illumina sequencing platform; the latest laboratory and bioinformatics protocols are
293 available at https://github.com/z0on/2bRAD_GATK. BcgI restriction enzyme was used and the
294 samples retained for this analysis had 2.3-20.2 (median: 7.45) million reads after trimming and
295 quality filtering (no duplicate removal was yet implemented in this 2bRAD version). The reads
296 were mapped to the genome of the outgroup species, *Acropora digitifera* (31, 32), to polarize the
297 allelic states into ancestral (as in *A. digitifera*) and derived, e.g., (33, 34). Genotypes were called
298 using GATK pipeline (35).

299

300 Preliminary analysis of sample relatedness using vcftools (36) revealed that our samples included
301 several clones: four repeats of the same genotype from the Keppel Island (van Oppen et al (9)
302 samples K210, K212, K213 and K216), another duplicated genotype from Keppel (samples K211
303 and K219), and one duplicated genotype from Magnetic Island (samples M16 and M17). All
304 other samples were unrelated. We took advantage of these clonal replicates to extract SNPs that
305 were genotyped with 100% reproducibility across replicates and, in addition, appeared as
306 heterozygotes in at least two replicate pairs (script replicatesMatch.pl with hetPairs=2 option).
307 These 7,904 SNPs were used as “true” SNP dataset to train the error model to recalibrate variant
308 quality scores at the last stage of the GATK pipeline. During recalibration, we used the transition-
309 transversion (Ts/Tv) ratio of 1.438 determined from the “true” SNPs to assess the number of false
310 positives at each filtering threshold (as it is expected that an increase of false positive calls would
311 decrease the Ts/Tv ratio towards unity). We chose the 95% tranche, with novel Ts/Tv = 1.451.
312 After quality filtering that restricted the calls to only bi-allelic polymorphic sites, retained only
313 loci genotyped in 95% or more of all individuals, and removed loci with the fraction of

314 heterozygotes exceeding 0.6 (possible lumped paralogs), we ended up with 25,090 SNPs. In total,
315 2bRAD tags interrogated 0.18% of the genome. The genotyping accuracy was assessed based on
316 the match between genotyped replicates using script repMatchStats.pl. Overall agreement
317 between replicates was 98.7% or better with the heterozygote discovery rate (fraction of matching
318 heterozygote calls among replicates) exceeding 96%.

319

320 *Genome-wide genetic divergence*

321

322 To begin to characterize genome-wide divergence between populations we used pairwise
323 genome-wide Weir and Cockerham's F_{ST} calculated by vcftools (36), principal component
324 analysis (PCA) using R package adegenet (37), and ADMIXTURE (38). For PCA and
325 ADMIXTURE, the data were thinned to keep SNPs separated by 5kb on average and by at least
326 2.5 kb, choosing SNPs with highest minor allele frequency (script thinner.pl with options
327 'interval=5000 criterion=maxAF').

328

329 *Demographic analysis and bootstrapping*

330

331 Prior to demographic analysis, Bayescan (39) was used to identify sites potentially under
332 divergent selection among populations, and 13 such sites with q-value <0.05 were removed.
333 Demographic models were fitted to 120 bootstrapped datasets, which were generated in two
334 stages. First, five alternatively thinned datasets were generated for which SNPs were randomly
335 drawn to be on average 5 kb apart and not closer than 2.5 kb. This time the SNPs were drawn at
336 random to avoid distorting the allele frequency spectrum unlike thinning for PCA and
337 ADMIXTURE where the highest minor allele frequency SNPs were selected. Then, 20
338 bootstrapped replicates were generated for each thinned dataset by resampling contigs of the
339 reference genome with replacement (script dadiBoot.pl). The fitted model parameters were
340 summarized after excluding bootstrap replicates that fell into the lowest 15% likelihood quantile
341 and the ones where model fitting failed to converge, leading to some parameters being
342 undetermined or at infinity (less than 10% of total number of runs). Delta-AIC values were
343 calculated for each bootstrap replicate that passed these criteria for both compared models, and
344 summarized to obtain bootstrap support value, the percentage of replicates favoring the
345 alternative model. While fitting *dadi* models, the data for each population were projected to
346 sample sizes maximizing the number of segregating sites in the analysis, resulting in 7000-8172
347 segregating sites per population.

348

349 *Unit conversion*

350

351 To convert *dadi*-reported coalescent parameter values (θ , T and M) into time in years (t), effective
352 population sizes in number of individuals (N_e) and migration rates as fraction of new immigrants
353 per generation (m), we estimated the mutation rate (μ) from the time-resolved phylogeny of

354 *Acorpora* genus based on *paxC* intron (40), at $4e-9$ per base per year. Although *A. millepora* was
355 shown to start reproducing in 3 years (17) we assumed the generation time of 5 years reasoning
356 that it would better reflect the attainment of full reproductive potential as the colony grows.
357 Assuming a genome size of $5e+8$ bases (31) the number of new mutations per genome per
358 generation is 10. Since the fraction 2bRAD-sequenced genome in our experiment was $1.8e-3$, the
359 mutation rate per 2bRAD-sequenced genome fraction per generation is $\mu = 0.018$. This value was
360 used to obtain:

- 361 - Ancestral effective population size: $Ne = \theta / 2\mu$
- 362 - Migration rate: $m = M / 2Ne$
- 363 - Time in years: $t = 2TNe \cdot 5$

364

365 *Biophysical model*

366

367 A spatially-explicit biophysical modeling framework (11, 41) was used to quantify migration
368 between coral reef habitats of the broader region surrounding the Great Barrier Reef, thereby
369 revealing the location, strength, and structure of a species' potential population connectivity. The
370 model's spatial resolution of ca. 8 km coincides with hydrodynamic data for the broader region
371 ($1/12.5$ degree; HYCOM+NCODA Reanalysis and Analysis product; hycom.org). Our
372 biophysical dispersal model relies on geographic data describing the seascape environment and
373 biological parameters capturing coral-specific life-histories. Coral reef habitat data are available
374 from the UNEP World Conservation Monitoring Centre (UNEP-WCMC; <http://data.unep-wcmc.org/datasets/1>) representing a globally-consistent and up-to-date representation of coral
375 reef habitat. To capture specific inter-annual variability, two decades of hydrodynamic data were
376 used from 1992 to 2013 (42).

377

378
379 Coral-specific biological parameters for *A. millipora* included relative adult density (dependent
380 on the habitat), reproductive output, larval spawning time and periodicity (e.g., Magnetic Island
381 populations spawn a month earlier than the other GBR sites (43)), maximum dispersal duration,
382 pre-competency and competency periods, and larval mortality (44, 45). The spatially explicit
383 dispersal simulations model the dispersal kernel (2-D surface) as a 'cloud' of larvae, allowing it
384 to be concentrated and/or dispersed as defined by the bio-physical parameters. An advection
385 transport algorithm is used for moving larvae within the flow fields (46).

386

387 Simulations were carried out by releasing a cloud of larvae into the model seascape at all
388 individual coral reef habitat patches and allowing the larvae to be transported downstream by the
389 currents. Ocean current velocities, turbulent diffusion, and larval behavior move the larvae
390 through the seascape at each time-step. Larval competency, behavior, density, and mortality
391 determine when and what proportion of larvae settle in habitat cells at each time step. When
392 larvae encounter habitat, the concentration of larvae settling with the habitat is recorded at that
393 time-step. From the dispersal data, we derived the coral migration matrix representing the

394 proportion of settlers to each destination patch that came from a source patch, which is analogous
395 to the source distribution matrix (47) and is equivalent to migration matrices derived from
396 population genetic analysis. It is important to note that migration matrices extracted for the field
397 sites represent the potential migration through all possible stepping-stones.

398

399 *Metapopulation adaptation model*

400

401 The model was implemented in SLiM the forward evolutionary simulator, by modifying the
402 provided recipe “Quantitative genetics and phenotypically-based fitness”. The model simulates
403 Fisher-Wright populations with discrete generations. At the start of the simulation, populations
404 were established at specified population sizes and pairwise migration rates (genetic replacement
405 rates), and all QTLs in all individuals were given a mutation with the effect size drawn from a
406 normal distribution with mean zero and specified standard deviation, to create standing genetic
407 variation. The phenotype of each individual was calculated as the sum of QTL effects plus
408 random noise to simulate desired heritability. Then, fitness of each individual was calculated
409 based on the difference between the individual’s phenotype (thermal optimum), temperature of
410 the environment, and the setting for phenotypic plasticity, modeled as the standard deviation of
411 the Gaussian slope of fitness decline with increasing distance between phenotype and
412 environment. Then, parents were chosen to produce the next generation according to their fitness;
413 parents for immigrant individuals are chosen from among individuals in the source population.
414 New mutations at QTLs happened at the specified rate when transitioning to the next generation
415 and the effect of a new mutation replaced the previous QTL effect.

416

417 Our code was designed for general modeling of multilocus adaptation in metapopulations and can
418 be customized easily. It is possible to adjust:

419

- 420 - Number of populations, their sizes, and pairwise migration rates. We modeled our five
421 populations with effective population sizes and pairwise migration rates inferred by *dadi*.
- 422 - Number of QTLs and the distribution of their effect sizes. To keep the model conservative,
423 we modeled only ten QTLs with normal distribution of effect sizes with a standard deviation
424 of 0.2°C. With ten QTLs, this setting implied that at the start of simulation only about 2% of
425 corals deviated from mean thermal tolerance by more than 1.5°C in either direction. Since
426 thermal differences between our populations exceeded 3°C, this narrow variation made local
427 adaptation rather non-trivial.
- 428 - Dominance of QTLs (set to 0.5 in our simulation).
- 429 - Phenotypic plasticity. We modeled three plasticity settings, 0.5, 1 and 2, which corresponded
430 to 86%, 40% and 13% fitness drop when the individual’s phenotypic optimum (calculated
431 based on QTLs and heritability setting) mismatched the environment by 1°C.

- 432 - Heritability (proportion of phenotypic variation explained by genetics). We examined values
433 1, 0.5, 0.25 and 1e-5, the latter to confirm that no adaptation or evolution was observed when
434 the trait was not heritable.
- 435 - Mutation rate, which was set to zero because we wanted to explore only the role of standing
436 genetic variation.
- 437 - Environmental changes, modeled as identical trends across populations with population-
438 specific offsets. The trends can be any combination of linear, cyclical and random
439 components. In the current simulation, environmental trends were offset by +1.6°C in Wilkie
440 and Magnetic populations and by -1.8°C in the Keppel population, to model differences in
441 midsummer monthly mean temperature among populations (Fig. 1). The trends included
442 only random thermal anomalies (drawn from a normal distribution with a standard deviation
443 of 0.25°C, to approximate ENSO events) for the first 2000 generations, after which a linear
444 increase at 0.05°C per generation was added to simulate warming.

445

446 To better model population dynamics, we implemented linear scaling of the population size and
447 immigration rates with the population's mean fitness post pre-adaptation period (the initial 2000
448 generations with no linear change in environment). In this way, a population declining in fitness
449 shrinks in size and stops contributing migrants to other populations.

450

451 All combinations of parameter settings were run ten times to ensure consistency. We found that
452 with population sizes in thousands, such as in our case, the results were very consistent among
453 independent runs. We therefore did not aggregate results over many replicated runs but show one
454 randomly chosen run for each tested parameter combination.

455

456 **Acknowledgements**

457

458 We wish to thank Ryan Gutenkunst and Benjamin Haller for their continuous support of *dadi* and
459 SLiM users, respectively. The bioinformatics analysis was accomplished using computational
460 resources of the Texas Advanced Computer Center. This study has been supported by NSF
461 (DEB-1054766) grant to M.V.M, ARC (LP120200245) and University of Melbourne ECR grants
462 to E. A.T., a Coral Reef Alliance grant ("Coral Adaptation Challenge") to E.A.T and M.V.M,
463 Queensland Government funding to L.K.B and AIMS funding to L.K.B. and M.J.V.O

464 **Data and code availability**

465 The finalized genotyping dataset in VCF format, detailed bioinformatic walkthrough, accessory
466 formatting and plotting scripts, *dadi* scripts and the SLiM model code are available from
467 <https://github.com/z0on/Adaptive-pathways-of-coral-populations-on-the-Great-Barrier-Reef>. Raw
468 sequencing data has been deposited to National Center for Biotechnology Information's Short
469 Reads Archive (accession number pending).

470

471 **References**

472

- 473 1. A. C. Baker, P. W. Glynn, B. Riegl, Climate change and coral reef bleaching: An ecological
474 assessment of long-term impacts, recovery trends and future outlook. *Estuar. Coast. Shelf Sci.* **80**,
475 435–471 (2008).
- 476 2. T. P. Hughes *et al.*, Climate change, human impacts, and the resilience of coral reefs. *Science*. **301**,
477 929–933 (2003).
- 478 3. J. M. Pandolfi, S. R. Connolly, D. J. Marshall, A. L. Cohen, Projecting coral reef futures under
479 global warming and ocean acidification. *Science*. **333**, 418–22 (2011).
- 480 4. G. B. B. Dixon *et al.*, Genomic determinants of coral heat tolerance across latitudes. *Science*. **348**,
481 1460–1462 (2015).
- 482 5. P. K. Ingvarsson, Restoration of genetic variation lost – the genetic rescue hypothesis. *Trends Ecol.*
483 *Evol.* **16**, 62–63 (2001).
- 484 6. G. De’ath, K. E. Fabricius, H. Sweatman, M. Puotinen, The 27-year decline of coral cover on the
485 Great Barrier Reef and its causes. *Proc. Natl. Acad. Sci. U. S. A.* **109**, 17995–9 (2012).
- 486 7. S. Wang, E. Meyer, J. K. McKay, M. V Matz, 2b-RAD: a simple and flexible method for genome-
487 wide genotyping. *Nat. Methods*. **9**, 808–810 (2012).
- 488 8. M. J. H. van Oppen, V. Lukoschek, R. Berkelmans, L. M. Peplow, A. M. Jones, A population
489 genetic assessment of coral recovery on highly disturbed reefs of the Keppel Island archipelago in
490 the southern Great Barrier Reef. *PeerJ*. **3**, e1092 (2015).
- 491 9. M. J. H. Van Oppen, L. M. Peplow, S. Kininmonth, R. Berkelmans, Historical and contemporary
492 factors shape the population genetic structure of the broadcast spawning coral, *Acropora millepora*,
493 on the Great Barrier Reef. *Mol. Ecol.* **20**, 4899–4914 (2011).
- 494 10. R. N. Gutenkunst, R. D. Hernandez, S. H. Williamson, C. D. Bustamante, Inferring the joint
495 demographic history of multiple populations from multidimensional SNP frequency data. *PLoS*
496 *Genet.* **5**, e1000695 (2009).
- 497 11. E. A. Treml, J. Roberts, P. N. Halpin, H. P. Possingham, C. Riginos, The emergent geography of
498 biophysical dispersal barriers across the Indo-West Pacific. *Divers. Distrib.* **21**, 465–476 (2015).
- 499 12. E. A. Treml *et al.*, Reproductive Output and Duration of the Pelagic Larval Stage Determine
500 Seascape-Wide Connectivity of Marine Populations. *Integr. Comp. Biol.* **52**, 525–537 (2012).
- 501 13. J. Lough, A. Hobday, Observed climate change in Australian marine and freshwater environments.
502 *Mar. Freshw. Res.* **62**, 984–999 (2011).
- 503 14. B. Charlesworth, Fundamental concepts in genetics: Effective population size and patterns of
504 molecular evolution and variation. *Nat. Rev. Genet.* **10**, 195–205 (2009).
- 505 15. W. Renema *et al.*, Are coral reefs victims of their own past success? *Sci. Adv.* **2**, e1500850 (2016).
- 506 16. B. C. Haller, P. W. Messer, SLiM 2: Flexible, interactive forward genetic simulations. *Mol. Biol.*
507 *Evol.* **34**, 230–240 (2017).
- 508 17. M. Vanessa, B. Baria, D. W. Dela Cruz, R. D. Villanueva, J. R. Guest, Spawning of three-year-old
509 *Acropora millepora* corals reared from larvae in Northern Philippines. *Bull. Mar. Sci.* **88**, 61–62
510 (2012).
- 511 18. IPCC, *Climate Change 2007 - The Physical Science Basis. Contribution of Working Group I to the*
512 *Fourth Assessment Report of the IPCC* (Cambridge University Press, New York, NY, 2007).
- 513 19. R. Berkelmans, M. J. H. van Oppen, The role of zooxanthellae in the thermal tolerance of corals: a
514 “nugget of hope” for coral reefs in an era of climate change. *Proc. R. Soc. B-Biological Sci.* **273**,
515 2305–2312 (2006).
- 516 20. A. H. Baird, J. R. Guest, B. L. Willis, Systematic and biogeographical patterns in the reproductive
517 biology of scleractinian corals. *Annu. Rev. Ecol. Evol. Syst.* **40**, 551–571 (2009).
- 518 21. K. Quigley, B. Willis, L. Bay, Heritability of the Symbiodinium community in vertically- and
519 horizontally-transmitting broadcast spawning corals. *bioRxiv*. doi: <https://doi.org/10.1101/100453>
520 (2017).

- 521 22. E. J. Howells *et al.*, Coral thermal tolerance shaped by local adaptation of photosymbionts. *Nat.*
522 *Clim. Chang.* **2** (2011), pp. 116–120.
- 523 23. F. P. Palstra, D. J. Fraser, Effective/census population size ratio estimation: a compendium and
524 appraisal. *Ecol. Evol.* **2**, 2357–2365 (2012).
- 525 24. S. R. Palumbi, D. J. Barshis, N. Traylor-Knowles, R. A. Bay, Mechanisms of reef coral resistance
526 to future climate change. *Science*. **344**, 895–8 (2014).
- 527 25. E. J. Howells, R. Berkelmans, M. J. H. van Oppen, B. L. Willis, L. K. Bay, Historical thermal
528 regimes define limits to coral acclimatization. *Ecology*. **94**, 1078–1088 (2013).
- 529 26. D. Nettle, M. Bateson, Adaptive developmental plasticity: what is it, how can we recognize it and
530 when can it evolve? *Proc. R. Soc. B Biol. Sci.* **282**, 20151005 (2015).
- 531 27. Great Barrier Reef Marine Park Authority, *Interim report on the environmental impacts of the 2016*
532 *coral bleaching event*.
- 533 28. O. Hoegh-Guldberg *et al.*, Assisted colonization and rapid climate change. *Science*. **321**, 345–346
534 (2008).
- 535 29. S. N. Aitken, M. C. Whitlock, Assisted Gene Flow to Facilitate Local Adaptation to Climate
536 Change. *Annu. Rev. Ecol. Evol. Syst.* **44**, 367–388 (2013).
- 537 30. G. B. Dixon, L. K. Bay, M. V. Matz, Bimodal signatures of germline methylation are linked with
538 gene expression plasticity in the coral *Acropora millepora*. *BMC Genomics*. **15**, 1109 (2014).
- 539 31. C. Shinzato *et al.*, Using the *Acropora digitifera* genome to understand coral responses to
540 environmental change. *Nature*. **476**, 320–U82 (2011).
- 541 32. M. J. H. van Oppen, B. J. McDonald, B. Willis, D. J. Miller, The Evolutionary History of the Coral
542 Genus *Acropora* (Scleractinia, Cnidaria) Based on a Mitochondrial and a Nuclear Marker:
543 Reticulation, Incomplete Lineage Sorting, or Morphological Convergence? *Mol. Biol. Evol.* **18**,
544 1315–1329 (2001).
- 545 33. B. F. Voight, S. Kudaravalli, X. Wen, J. K. Pritchard, A map of recent positive selection in the
546 human genome. *PLoS Biol.* **4**, e72 (2006).
- 547 34. I. K. Jordan *et al.*, A universal trend of amino acid gain and loss in protein evolution. *Nature*. **433**,
548 633–8 (2005).
- 549 35. A. Mckenna *et al.*, The Genome Analysis Toolkit: A MapReduce framework for analyzing next-
550 generation DNA sequencing data. *Genome Res.* **20**, 1297–1303 (2010).
- 551 36. P. Danecek *et al.*, The variant call format and VCFtools. *Bioinformatics*. **27**, 2156–8 (2011).
- 552 37. T. Jombart, adegenet: a R package for the multivariate analysis of genetic markers. *Bioinformatics*.
553 **24**, 1403–5 (2008).
- 554 38. D. H. Alexander, J. Novembre, K. Lange, Fast model-based estimation of ancestry in unrelated
555 individuals. *Genome Res.* **19**, 1655–64 (2009).
- 556 39. T. Günther, G. Coop, Robust identification of local adaptation from allele frequencies. *Genetics*.
557 **195**, 205–20 (2013).
- 558 40. Z. T. Richards, D. J. Miller, C. C. Wallace, Molecular phylogenetics of geographically restricted
559 *Acropora* species: Implications for threatened species conservation. *Mol. Phylogenet. Evol.* **69**,
560 837–851 (2013).
- 561 41. E. A. Treml, P. N. Halpin, D. L. Urban, L. F. Pratson, Modeling population connectivity by ocean
562 currents, a graph-theoretic approach for marine conservation. *Landscape Ecol.* **23**, 19–36 (2008).
- 563 42. E. P. Chassignet *et al.*, The HYCOM (HYbrid Coordinate Ocean Model) data assimilative system.
564 *J. Mar. Syst.* **65**, 60–83 (2007).
- 565 43. R. C. Babcock *et al.*, Synchronous Spawnings of 105 Scleractinian Coral Species on the Great-
566 Barrier-Reef. *Mar. Biol.* **90**, 379–394 (1986).
- 567 44. S. W. Davies, E. A. Treml, C. D. Kenkel, M. V. Matz, Exploring the role of Micronesian islands in
568 the maintenance of coral genetic diversity in the Pacific Ocean. *Mol. Ecol.* **24**, 70–82 (2015).
- 569 45. S. R. Connolly, A. H. Baird, Estimating dispersal potential for marine larvae: dynamic models
570 applied to scleractinian corals. *Ecology*. **91**, 3572–3583 (2010).

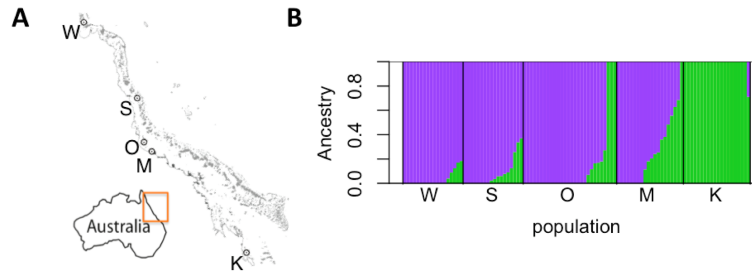
- 571 46. P. K. Smolarkiewicz, J. Szmelter, An MPDATA-based solver for compressible flows. *Int. J.*
572 *Numer. Methods Fluids*. **56**, 1529–1534 (2008).
573 47. R. K. Cowen, G. Gawarkiewicz, J. Pineda, S. Thorrold, F. Werner, Population Connectivity in
574 Marine Systems: An Overview. *Oceanography*. **20**, 14–21 (2007).
575

576 **Supplemental Figures**

577

578

579



580

581

582

583

584

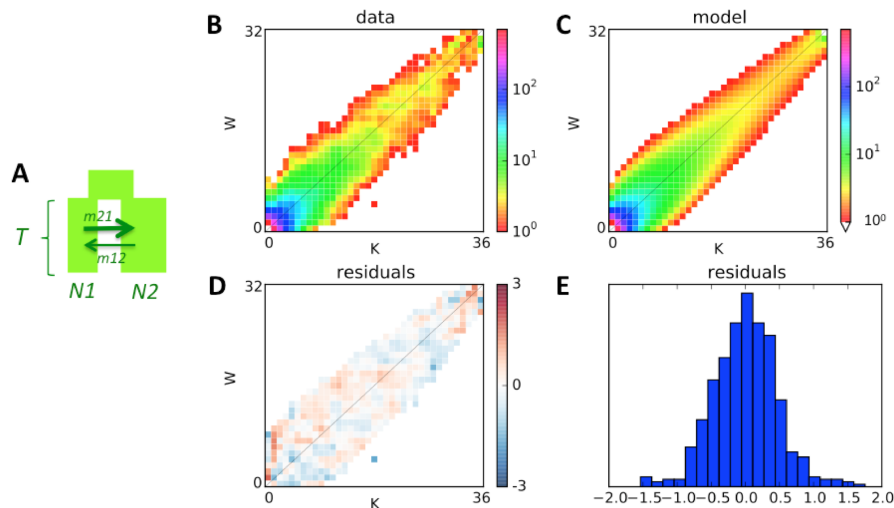
585

586

587

588

Figure S1. ADMIXTURE analysis of genetic differentiation between populations. (A) Map of sampled locations with one-letter population identifiers. (B) ADMIXTURE plot of ancestry proportions with $K = 2$ (optimal K was 1).



589

590

591

592

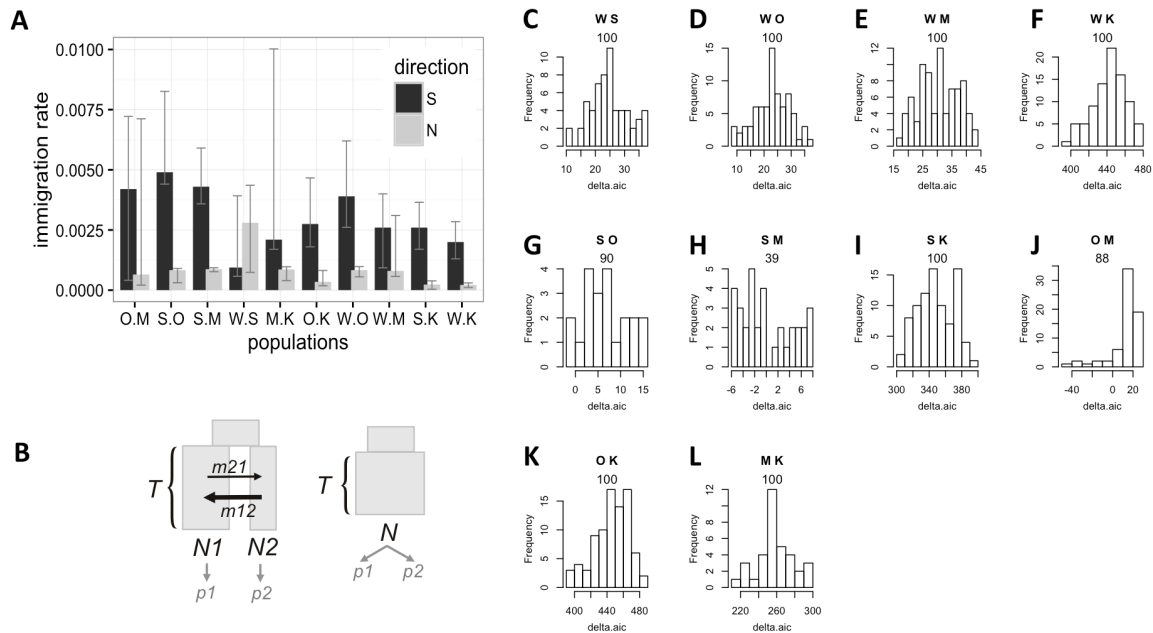
593

594

595

Figure S2. Example of two-population *dadi* model fit. (A) The model: ancestral population splits into two populations of unequal sizes ($N1$ and $N2$) some time T in the past, which exchange migrants with different rates depending on direction. (B) Observed allele frequency spectrum comparing Wilkie (W) and Keppel (K) populations. (C) Allele frequency spectrum generated by the fitted model. (D, E) Map and histogram of residuals (absolute scale).

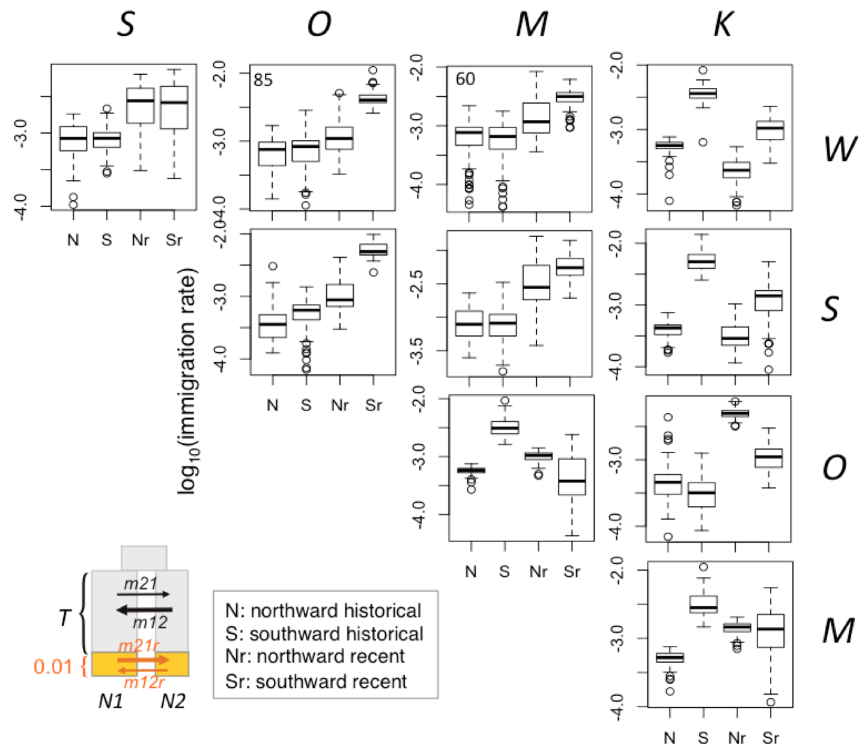
596
597
598



599
600
601
602
603
604
605
606
607
608
609
610
611
612

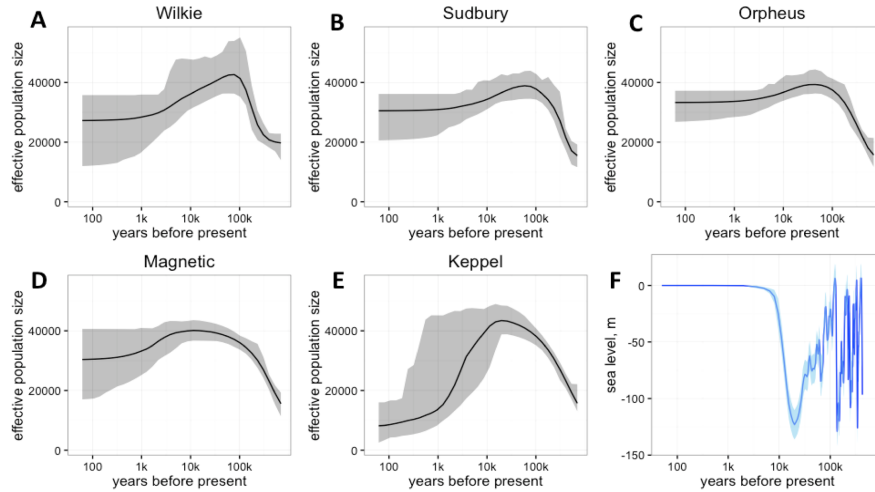
Figure S3. Bootstrap analysis of migration rates and population subdivision using *dadi*. (A) Migration among population pairs, with bootstrap-derived 95% confidence intervals. The pairs are identified on the x-axis and sorted by increasing geographical distance. Black bars – southward migration, grey bars – northward migration. (B) Models being compared: the full model (left) implies populations’ split into two different sizes ($N1$ and $N2$) at time T in the past, since when they exchanged migrants at unequal rates depending on direction. Reduced model allows for population size change at time T in the past but does not include population split: the two genotyped groups ($p1$ and $p2$) are regarded as two samples from the same population. (C-L) Histograms of delta-AIC values for 100 bootstrap replicates (bootstrap was performed over genomic contigs of the draft genome of *A. digitifera*). Positive numbers indicate support for the full model. The letters on top of each panel identify compared populations, the number is the proportion of positive bootstrap replicates (i.e., bootstrap support for the full model). The only comparison that did not receive >50% bootstrap support for population split is between S and M populations (panel H).

613
614
615
616



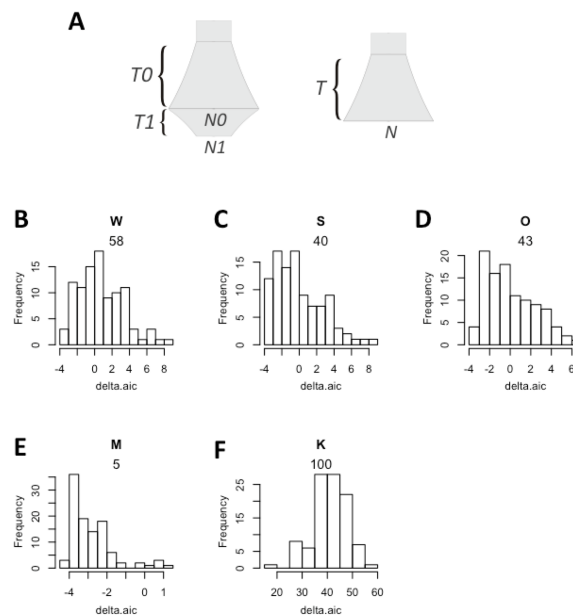
617
618
619
620
621
622
623
624
625
626
627
628

Figure S4. Migration rates inferred by the *dadi* model allowing for the change in migration rates over the last 0.01 T units (15-20 generations or 75-100 years, in our case). Box plots show historical (N, S) and recent (Nr, Sr) migration rates inferred among pairs of population across 100 bootstrap replicates. Numbers in the top left corner of the WO and WM plots are delta-AIC bootstrap support values for the model with the recent change in migration when compared to the split-with-migration model with no recent change (Fig. 1A). All other pairs had less than 50% delta-AIC bootstrap support. There is no consistent recent change in the preferential direction of migration.



629
630
631
632
633

Figure S5. Population history. (A-E) Historical population sizes with bootstrap-derived 95% confidence intervals, according to the two-growth model (Fig. S6 A). (F) Sea level with shaded area corresponding to standard error (41).

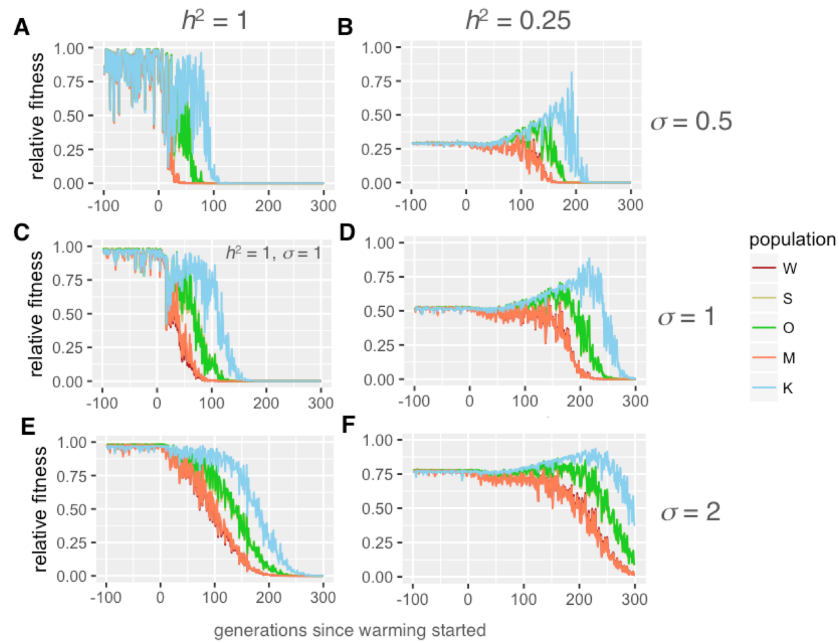


634
635
636
637
638
639
640
641

Figure S6. Delta-AIC bootstrap analysis of single-population models. (A) Models compared. The full model (left) includes two exponential growth periods (any of which could be growth or decline), the reduced model (right) has only one growth period. (B-F) Histograms of delta-AIC values for 100 bootstrap replicates. Positive numbers indicate support for the full model. The letter on top of each panel identify the population, the number is the proportion of positive bootstrap replicates (i.e., bootstrap support for the full model). The two-growth model is strongly supported for population K (panel F) and marginally supported for population W (panel B).

642

643



644

645

646

647

648

649

650

651

652

653

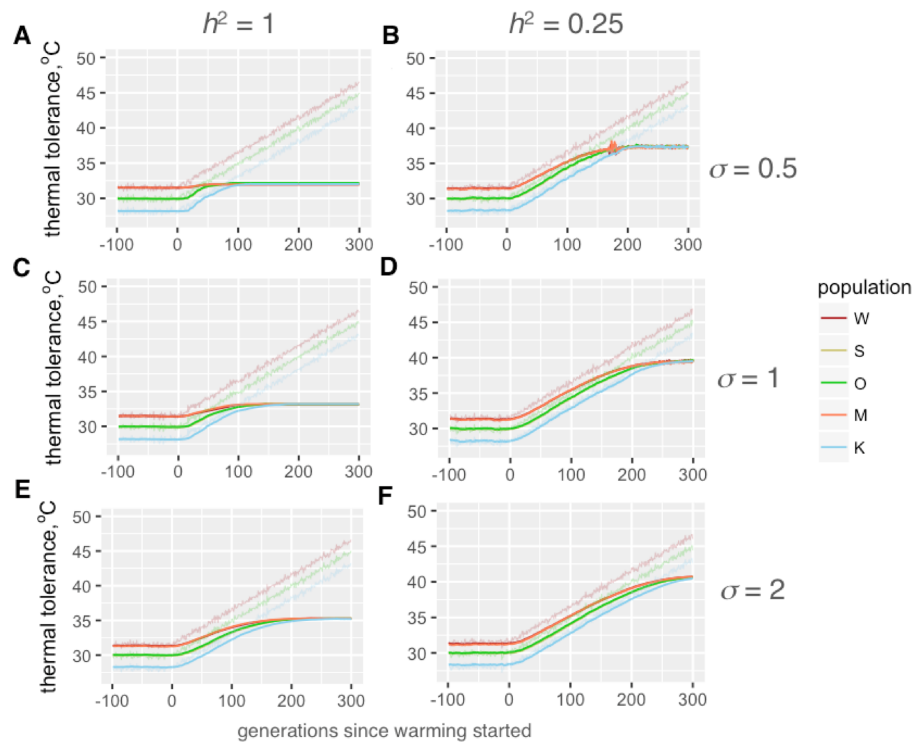
654

655

656

Figure S7. Fitness of modeled populations after pre-adaptation period and under warming, depending on heritability of thermal tolerance (h^2 , proportion of phenotypic variation explained by genetics) and phenotypic plasticity (σ , standard deviation of the Gaussian slope of fitness decline away from the phenotypic optimum, in degrees C). X-axis is generations; warming starts at generation 0. Y-axis is fitness relative to maximal fitness at the genetically determined optimum. Warm-adapted populations (W and M) are shown as red-tint traces, populations from mild thermal regime (S and O) are green-tint traces, and the cool-adapted population (K) is the blue trace. Pairs of traces for warm- and mild-adapted populations largely overlap. (A, C, E): $h^2=1$. (B, D, F): $h^2=0.25$. (A, B): $\sigma = 0.5$. (C, D): $\sigma = 1$. (E, F): $\sigma = 2$. Higher plasticity facilitates metapopulation persistence during warming and confers stability against random fluctuations. Higher plasticity also partially rescues the drop in fitness achievable under low heritability (compare pre-warming generations, from -100 to 0, on panels B, D and F).

657



658

659

660

661

662

663

664

665

666

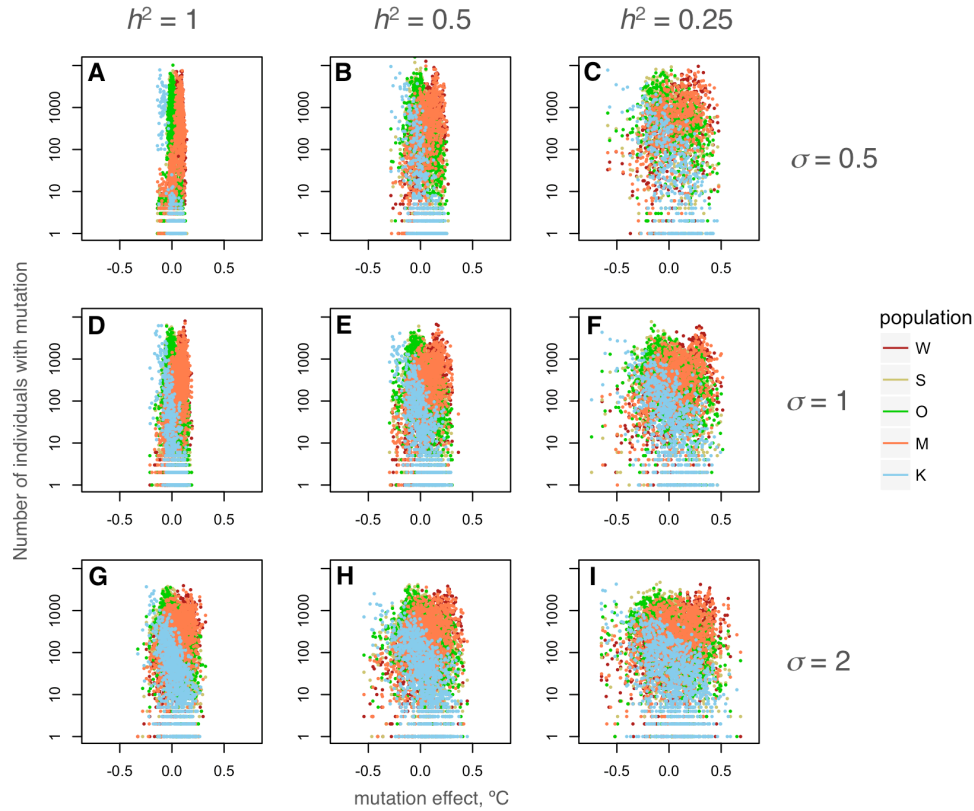
667

668

669

670

Figure S8. Higher plasticity and lower heritability promote longer and more extensive evolution in response to warming. The graphs show mean thermal tolerance of modeled populations after pre-adaptation period and under warming, depending on heritability of thermal tolerance (h^2 , proportion of phenotypic variation explained by genetics) and phenotypic plasticity (σ , standard deviation of the Gaussian slope of fitness decline away from the phenotypic optimum, in degrees C). X-axis is generations; warming starts at generation 0. Y-axis is thermal tolerance (mean phenotype of the population). Warm-adapted populations (W and M) are shown as red-tint traces, populations from mild thermal regime (S and O) are green-tint traces, and the cool-adapted population (K) is the blue trace. Thin noisy lines are modeled temperatures at the corresponding locations. Pairs of traces for warm- and mild-adapted populations largely overlap. (A, C, E): $h^2=1$. (B, D, F): $h^2=0.25$. (A, B): $\sigma = 0.5$. (C, D): $\sigma = 1$. (E, F): $\sigma = 2$.



671
672
673
674
675
676
677
678
679
680

Figure S9. Higher plasticity (σ) and lower heritability (h^2) promote retention of higher genetic variation in thermal tolerance. The scatterplots show the dependence of the number of individuals in a population bearing a mutation at a thermal QTL locus on the mutation's effect size (change in thermal tolerance, in °C) at the end of the pre-adaptation period (2000 generations with no directional change in temperature). The starting standing genetic variation was the same in all simulations. (A,D,E): $h^2=1$. (B,E,H): $h^2=0.5$. (C,F,I): $h^2=0.25$. (A-C): $\sigma = 0.5$. (D-F): $\sigma = 1$. (G-I): $\sigma = 2$. Populations are colored according to the color scheme used in Figures 3, S9 and S10 (see legend).